



**Environmental  
Science**  
Nano

**Delineating the Role of Surface Grafting Density of Organic Coatings on the Colloidal Stability, Transport, and Sorbent Behavior of Engineered Nanoparticles**

Journal:	<i>Environmental Science: Nano</i>
Manuscript ID	EN-ART-06-2023-000358.R1
Article Type:	Paper

**SCHOLARONE™**  
Manuscripts

## Environmental Significance Statement

Nanoparticle behavior in water is governed by surface properties, including effective surface-based coatings. Here we quantitatively describe the critical role of surface coatings with regard to grafting density of the stabilizing organic layer (i.e. number of stabilizing agents per surface area), on the aggregation, transport, and sorption behavior of engineered nanoparticles. For these, we explore particle behavior in relevant water chemistries, including the role of natural organic matter.

1  
2  
3  
4 Delineating the Role of Surface Grafting Density of Organic  
5  
6  
7  
8 Coatings on the Colloidal Stability, Transport, and Sorbent  
9  
10  
11 Behavior of Engineered Nanoparticles  
12  
13  
14  
15  
16  
17

18 *Junseok Lee,<sup>a</sup> Changwoo Kim,<sup>b</sup> Daniel Schmucker,<sup>c</sup> Seung Soo Steve Lee,<sup>a</sup> Shuchi Liao,<sup>d</sup> Kurt*  
19  
20 *D. Pennell,<sup>d</sup> and John D. Fortner<sup>\*a</sup>*  
21  
22

23  
24 <sup>a</sup>Department of Chemical and Environmental Engineering, Yale University, New Haven, CT,  
25  
26 06511 United States  
27

28  
29 <sup>b</sup>School of Earth Sciences and Environmental Engineering, Gwangju Institute of Science and  
30  
31 Technology, Gwangju 61005, Republic of Korea  
32  
33

34  
35 <sup>c</sup>Department of Energy, Environmental and Chemical Engineering, Washington University in St.  
36  
37 Louis, St. Louis, MO, 63130 United States  
38  
39

40  
41 <sup>d</sup>School of Engineering, Brown University, Providence, RI, 02912 United States  
42

43  
44 \*To whom correspondence should be addressed:  
45

46  
47 John D. Fortner: Tel: +1-314-935-9293; Email: [john.fortner@yale.edu](mailto:john.fortner@yale.edu)  
48  
49

50  
51  
52  
53 **Keywords**  
54

55  
56 Surface grafting density; colloidal stability; aggregation and deposition; transport; sorption  
57  
58  
59  
60

**Abstract**

Aqueous stability and sorption affinity (towards target environmental contaminants) of engineered nanoparticles, composed of inorganic nanoparticles and surface stabilizers, underpin their environmental behavior and application potential for a variety of proposed technologies. However, fundamentally delineating the role of surface coatings (in terms of surface coating density) remains outstanding for a number of particle systems. To address this critical issue, we describe colloidal stability, transport, and sorption behavior of engineered manganese oxide nanoparticles as a function of specific surface grafting density. We observed higher grafting density results in higher colloidal stability due to higher steric repulsion forces. Additionally, humic acid (HA) significantly improved the stability of NPs with lower grafting density, while showing negligible effects in higher grafting density. Deposition behavior did not correlate with grafting density, regardless of organic coating types. In the presence of HA, deposition behavior of negatively charged NPs was not altered, while deposition of positively charged NPs was dependent on HA presence. Higher grafting density of CTAB also enhanced chromate sorption capacity due to the increasing number of favorable functional groups. Taken together, this work clearly demonstrates the critical need to fully understand NP surface coating dynamics as they relate to fundamental material behavior and performance.

## Introduction

Modification of engineered nanoparticles (NPs) surfaces with organic surfactants has received considerable attention in recent years.<sup>1-3</sup> Surface functionalization of NPs not only enhances the physicochemical and mechanical properties, but also improves their biocompatibility.<sup>4</sup> For example, NP surface functionalization can improve colloidal stability of NPs in water,<sup>5, 6</sup> preventing dissolution,<sup>7</sup> enhance reactivity/remediation of potentially harmful substances,<sup>8, 9</sup> and even mitigate toxicity.<sup>10</sup> Additionally, as the production and applications of engineered NPs continues to increase, the corresponding potential for environmental exposure is also increased, furthering the need to fundamentally predict NP behavior.

Following intentional or accidental release of engineered NPs into the environment, their fate and transport are largely governed by particle–particle and particle–surface interactions, and thus, when present, surface (organic) NP coating plays a critical role. For instance, He et al. observed that zerovalent iron NPs coated with carboxymethyl cellulose exhibited enhanced transport behavior in a simulated aquifer because due to surface-based electrostatic stabilization (preventing the NPs aggregation and deposition).<sup>11</sup> Phenrat et al. showed that dispersion stability of zerovalent iron NPs was enhanced by surface modification via polyelectrolytes when compared to ‘bare’ NPs.<sup>12</sup> Li et al. reported that silver NPs coated with Tween 80 were significantly more stable than uncoated silver NPs.<sup>13</sup> When considering specific surface coating properties, the grafting density of organic molecules on the surface is a crucial, yet often under studied (and under reported), factor governing the magnitude of both electrostatic and steric repulsion forces related to aggregation and deposition behavior(s).<sup>14</sup>

Organic coatings also affect the sorption behavior of engineered NPs via specific affinity

1  
2  
3  
4 between organic coated NPs and target contaminants. For example, Lee et al. demonstrated that  
5  
6 phosphonic acid group on manganese ferrite NPs showed highest sorption capacity for uranium  
7  
8 removal rather than positively charged surface coating.<sup>15</sup> Kim et al. showed that iron oxide NPs  
9  
10 with positively charged surface coatings have higher sorption capacity for arsenic and chromium  
11  
12 sorption compared to negatively charged NPs.<sup>16</sup> Huang and Keller revealed that magnetic NPs  
13  
14 functionalized with EDTA showed high sorption capacity for heavy metal removal for variety of  
15  
16 water chemistries as well as material regeneration.<sup>17</sup> Among these and numerous other studies,  
17  
18 it is clear that surface coating density is a critical NP design criterion,<sup>18-20</sup> yet remains relatively  
19  
20 understudied.  
21  
22  
23  
24

25  
26 While there are many reports on NP surface coatings,<sup>21</sup> direct evaluation of NP behavior(s)  
27  
28 as a function of surface coating density has not been extensively investigated due to the required  
29  
30 synthesis precision and associated (and incomparable) stability regimes. In this study, we  
31  
32 examined NP behavior as a function of carefully controlled grafting densities, comparing colloidal  
33  
34 stability, transport, and sorption behavior as well as exploring the influence/effects of natural  
35  
36 organic matter (NOM), as humic acid (HA). For this, we evaluated the effect of grafting density  
37  
38 on colloidal stability in terms of critical coagulation concentration (CCC), as quantified via  
39  
40 aggregation kinetics. Sand column tests were also performed and modeled to evaluate NP  
41  
42 deposition behavior as a function of grafting density and coating type, along with the presence of  
43  
44 HA. Lastly, sorption capacities for chromate (as an example inorganic pollutant) are  
45  
46 demonstrated as a function of surface coating grafting density.  
47  
48  
49  
50  
51  
52  
53

## 54 **Methods**

55  
56  
57  
58  
59  
60

## Materials

Manganese(II) chloride tetrahydrate ( $\text{MnCl}_2 \cdot 4\text{H}_2\text{O}$ , 99.99%), oleic acid (OA, 90%), 1-octadecene (90%), polyethyleneglycol (PEG, MW = 5000), cetyltrimethylammonium bromide (CTAB, 95%), hexane (98.5%), acetone (99.5%), ethanol (99.9%), sodium chloride (NaCl, 99%), calcium chloride ( $\text{CaCl}_2$ , 99%), nitric acid ( $\text{HNO}_3$ , 70%), sodium hydroxide (NaOH, 97%), sodium bicarbonate ( $\text{NaHCO}_3$ , 99.7%), potassium chloride (KCl, 99%), potassium bromide (KBr, 99.95%), potassium chromate ( $\text{K}_2\text{Cr}_2\text{O}_7$ , 99%), and humic acid (HA, technical grade) were purchased from Sigma-Aldrich. Sodium oleate (97%) was purchased from TCI America. Nitrogen gas ( $\text{N}_2$ , 99.999%, Airgas) was used to synthesize NPs.

## Preparation of manganese oxide nanoparticles

Manganese oxide ( $\text{Mn}_x\text{O}_y$ ) NPs were synthesized by thermal decomposition of manganese oleate as a  $\text{Mn}_x\text{O}_y$  precursor at 320°C. Detailed procedures for synthesis of manganese oleate and  $\text{Mn}_x\text{O}_y$  NPs were reported in previous studies.<sup>22, 23</sup> The synthesized NPs were purified over six times by centrifuging at 7000 rpm using acetone, ethanol, and hexane. The purified  $\text{Mn}_x\text{O}_y$  NPs were dispersed and stored in hexane. The resulting  $\text{Mn}_x\text{O}_y$  NPs were phase transferred using various surface stabilizing agents, such as OA, PEG, and CTAB ( $\text{Mn}_x\text{O}_y@OA$ ,  $\text{Mn}_x\text{O}_y@PEG$ , and  $\text{Mn}_x\text{O}_y@CTAB$ ). Different concentrations of stabilizing agent were mixed with 10 mL of ultrapure water (18.2 M $\Omega$  cm, Millipore) and 0.4 mL of  $\text{Mn}_x\text{O}_y$  NPs in hexane solution ( $2.2 \times 10^{14}$  NPs per liter) through probe sonication (UP50H, Hielscher) at 80% amplitude and full cycle for 10 min. The resulting solution (in an opened vial) were stored under the fume hood to remove the remaining hexane in solution for 24 h, and subsequently the residual of surface stabilizers in

1  
2  
3  
4 the solution was removed by ultrafiltration membrane (cellulose, 100 kDa MWCO, Millipore)  
5  
6 under stirring, followed by syringe filtration (0.22  $\mu\text{m}$  PES, Millipore).  
7  
8

9  
10 The grafting density on the NPs was determined using total organic carbon (TOC, TOC-  
11 L analyzer, Shimadzu Corporation) measurements. The number of organic molecules per NPs  
12 was quantified by difference of TOC values between the solution with the organic coated NPs and  
13 supernatant without the NPs removed by ultracentrifuge (Sorvall WX Ultra 80, Thermo Scientific)  
14 at 50000 rpm for 2 h, with assumption of equivalent distribution for organic molecules to the NPs.  
15  
16 The concentration of NPs was determined by digestion of NPs with hydrochloric acid (1 N) under  
17 heating (80°C) and measuring their manganese concentration using inductively coupled plasma-  
18 optical emission spectrometer (ICP-OES).  
19  
20  
21  
22  
23  
24  
25  
26  
27  
28  
29  
30

### 31 **Critical coagulation concentration (CCC)**

32  
33  
34 Aggregation kinetic of NPs was evaluated by measuring hydrodynamic diameter ( $D_H$ ) of  
35  $\text{Mn}_x\text{O}_y$  NPs (ca. 1 mg  $\text{L}^{-1}$  as Mn concentration) with different grafting densities in the absence and  
36 presence of HA as a function of NaCl and  $\text{CaCl}_2$  concentrations for 20 min. Their  $D_H$  was  
37 measured using a Malvern Nano ZS system by Malvern Panalytical (Malvern Zetasizer Nanoseries,  
38 Malvern, UK). All measurements were conducted at a room temperature of 22°C. The solution  
39 pH was adjusted to  $7.0 \pm 0.2$  with  $\text{HNO}_3$  and NaOH solutions. The colloidal stability of NPs  
40 having different grafting densities was evaluated by comparing CCC values in which the  
41 aggregation kinetic reached to diffusion-limited regimes (i.e., the attachment efficiency is equal to  
42 1). The attachment efficiency ( $\alpha$ ) for aggregated NPs was calculated by following equation:  
43  
44  
45  
46  
47  
48  
49  
50  
51  
52  
53  
54  
55  
56  
57  
58  
59  
60



$$\alpha = \frac{1}{W} = \frac{k}{k_{fast}} \quad (1)$$

where  $W$  is stability ratio,  $k$  is aggregation rate constant obtained at interested salt concentrations, and  $k_{fast}$  is diffusion-limited aggregation rate constant obtained under favorable aggregation conditions.<sup>24, 25</sup>

### Column experiments

Column experiments were performed in water saturated columns packed with 30-40 mesh Ottawa sand through glass column (Spectra/Chrom, TX) with dimensions of 15 cm in length and 1.5 cm in inner diameter. Prior to transport tests, the packed column was flushed with DI water and desired background solution. Following the saturation, a nonreactive tracer (KBr) test was performed to assess hydrodynamic properties of the porous media, and the resulting porosity was determined to be ca. 0.39. All experiments were conducted at 0.76 m/d of a pore-water velocity, in the range of typical values of real groundwater flow.<sup>26-28</sup> For NPs transport experiments, a 5 pore volume (PV) pulse of solution containing  $Mn_xO_y$  NPs with different grafting densities (1 mg  $L^{-1}$  as Mn concentration) under same background electrolyte composition was introduced to the column, followed by the injection of a NP-free background solution and DI water. Column effluent samples were collected continuously using fraction collector and NP concentration was measured by ICP-OES as described above. Following each transport experiments, the columns were sectioned into 5 increments, and retained NPs concentrations were extracted and measured using ICP-OES to assess their spatial distribution in the column. Detailed information about the column experiment methods are provided in the SI.

The resulting data of column tests were interpreted using clean-bed filtration theory (CFT)<sup>29</sup> and a modified filtration theory (MFT) approach.<sup>30</sup> In CFT, the attachment efficiency ( $\alpha$ ) of NPs to the sand was calculated by the following equation:

$$\alpha = -\frac{2}{3} \frac{d_c}{(1-\varepsilon)L\eta_0} \ln \frac{C_e}{C_0} \quad (2)$$

where  $d_c$  is diameter of sand [L],  $\varepsilon$  is porosity of packed column,  $L$  is length of the column [L],  $\eta_0$  is single collector efficiency,  $C_e$  is effluent concentration of NPs, and  $C_0$  is influent concentration of NPs [M/L<sup>3</sup>]. The single collector efficiency ( $\eta_0$ ) was numerically estimated using the empirical equation<sup>31</sup>:

$$\eta_0 = 2.4A_S^{1/3}N_R^{-0.081}N_{Pe}^{-0.715}N_{vdW}^{0.052} + 0.55A_SN_R^{1.675}N_A^{0.125} + 0.22N_R^{-0.24}N_G^{1.11}N_{vdW}^{0.053} \quad (3)$$

where  $A_S$  is Happel model parameter,  $N_R$  is aspect ratio,  $N_{Pe}$  is Peclet number,  $N_{vdW}$  is van der Waals number,  $N_A$  is attraction number, and  $N_G$  is gravitational number. Each term in above equation represents the three filtration mechanisms; diffusion, interception, and sedimentation, respectively. In the MFT approach, a traditional mass balance equation that accounts advection, hydrodynamic dispersion and particle deposition was solved to simulate NP effluent concentration and solid phase retention profiles:

$$\frac{\partial C}{\partial t} + \frac{\rho_b \partial S}{\theta_w \partial t} = D_h \frac{\partial^2 C}{\partial x^2} - v_p \frac{\partial C}{\partial x} \quad (4)$$

Here,  $C$  and  $S$  are the NP aqueous and solid-phase concentrations [M/L<sup>3</sup> and M/M] respectively;  $t$  is time [t],  $x$  is the distance from the column inlet [L];  $v_p$  is the average pore-water velocity [L/t],  $D_h$  is the hydrodynamic dispersion coefficient for the column [L<sup>2</sup>/t],  $\rho_b$  is the bulk density of the porous medium [M/L<sup>3</sup>], and  $\theta_w$  is the volumetric water content [L<sup>3</sup>/L<sup>3</sup>].

1  
2  
3  
4 For NP deposition, a Langmuir-type site block function was employed to describe the rate  
5 of attachment ( $k_{att}$ , 1/t) as attachment sites were occupied, and a first-order detachment term ( $k_{det}$ ,  
6  
7 1/t) was included to account for nanoparticle release<sup>32</sup>:  
8  
9

$$\frac{\rho_b \partial S}{\theta_w \partial t} = k_{att} \Psi C - \frac{\rho_b}{\theta_w} k_{det} S \quad (5)$$

$$\Psi = \frac{S_{max} - S}{S_{max}} \quad (6)$$

10  
11  
12  
13  
14  
15  
16  
17 Here,  $S_{max}$  is the maximum capacity of the solid phase for NP deposition. Equations 4-6  
18 were implemented to fit the NP effluent breakthrough curve (BTC) data using a central-in-space  
19 and fully implicit-in-time finite difference scheme in MATLAB R2022b (MathWorks, Natick,  
20 MA). The fitted parameters, including  $k_{att}$ ,  $k_{det}$  and  $S_{max}$ , are listed in Table S2. The NP  
21 retention profiles were then simulated using the fitted parameters.  
22  
23  
24  
25  
26  
27  
28  
29  
30  
31  
32

### 33 34 35 36 37 **Chromate sorption measurements**

38  
39  
40 The phase transferred  $Mn_xO_y$  NPs with different grafting densities (20 mg L<sup>-1</sup> as Mn  
41 concentration) were tested for chromate sorption (10 mg L<sup>-1</sup> as Cr(VI)) at pH 7. Chromate  
42 sorption dynamics was proceeded for 24 hours and the solution pH was adjusted to  $7.0 \pm 0.2$  twice  
43 (initially and after 4 h during each batch sorption experiment) using HNO<sub>3</sub> and NaOH solutions.  
44 After mixing for 24 h (equilibrium), the NPs were separated using ultracentrifuge at 50000 rpm  
45 for 2 h and remaining concentration of Cr(VI) in the supernatant was measured by ICP-OES. All  
46 experiments were performed in duplicate. The measured chromate sorption density (mass of  
47 adsorbed chromate per mass of  $Mn_xO_y$  NPs in the sample) was compared with respect to the  
48  
49  
50  
51  
52  
53  
54  
55  
56  
57  
58  
59  
60

grafting density of NPs.

## Results and discussion

### Characterization of manganese oxide nanoparticles with different grafting densities

Monodisperse manganese oxide ( $\text{Mn}_x\text{O}_y$ ) NPs were synthesized through thermal decomposition of manganese oleate at 320°C, resulting in highly crystalline NPs, stable in various nonpolar organic solvents such as, toluene and hexane (Fig. S1). As reported by our previous work,<sup>23</sup> synthesized  $\text{Mn}_x\text{O}_y$  NPs are demonstrated to be a core shell structure (a core particles of MnO with a thin shell of  $\text{Mn}_3\text{O}_4$  particles). We selected  $\text{Mn}_x\text{O}_y$  NPs due to our ability to precisely control particle shape and size during synthesis and for their antiferromagnetic property of core particle at room temperature, thus negating potential interfering magnetic effects.<sup>33</sup> Synthesized  $\text{Mn}_x\text{O}_y$  NPs ( $18.4 \pm 1.5$  nm) were then phase transferred into water via various surface coatings (i.e. stabilizing organic layer), including OA, CTAB, via ligand encapsulation method ( $\text{Mn}_x\text{O}_y@OA$ ,  $\text{Mn}_x\text{O}_y@CTAB$ ),<sup>34-36</sup> and PEG by ligand encapsulation ( $\text{Mn}_x\text{O}_y@PEG$ )<sup>20</sup> to render NPs hydrophilic and stable in aqueous media.

During the phase transfer process, we controlled the number of organic molecules per NPs (i.e., grafting density) by carefully controlling concentrations added during the final phase transfer step. The  $D_H$  of those phase-transferred NPs with different grafting densities is presented in Fig. 1. For the same surface coating, the  $D_H$  was consistent regardless of the grafting density, which indicates that the organic molecules on the outer-most layer were similarly oriented (e.g. no additional layering). The average  $D_H$  of organic functionalized NPs was around 25 to 31 nm for  $\text{MnO}@OA$ , 36 to 48 nm for  $\text{MnO}@PEG$ , and 27 to 41 nm for  $\text{MnO}@CTAB$ , in a wide range of

1  
2  
3  
4 grafting density, respectively. As shown in the figure, the bilayer coating structure with OA and  
5  
6 CTAB showed relatively small  $D_H$  rather compared with PEG coating(s), which is in line with our  
7  
8 previous studies.<sup>16, 23</sup> Zeta potential measurements of surface functionalized  $Mn_xO_y$  NPs (Fig.  
9  
10 S2) were  $-36$  to  $-34$  mV for  $MnO@OA$ ,  $-11$  to  $-28$  mV for  $MnO@PEG$ , and  $16$  to  $41$  mV for  
11  
12  $MnO@CTAB$ , which are also similar to our previous studies.<sup>15, 23, 34</sup>  
13  
14  
15  
16  
17  
18

### 19 **Colloidal stability**

20  
21  
22 Colloidal stability of the phase-transferred NPs was evaluated with respect to the grafting  
23  
24 density by measuring CCC values as a function of NaCl and  $CaCl_2$  concentrations. As shown in  
25  
26 Fig. 2, water stable NPs with various grafting density, were evaluated in mono- or di-valent  
27  
28 cationic salt solutions and their colloidal stability was monitored and compared as a function of  
29  
30 time. For these, the higher grafting density materials demonstrated higher stability, as larger  
31  
32 CCC values were observed for both NaCl and  $CaCl_2$  solutions (Fig. 2(a-d)). Specifically, CCC  
33  
34 values for higher grafting density of  $Mn_xO_y@OA$  (855 mM of NaCl and 21.8 mM of  $CaCl_2$ ) and  
35  
36  $Mn_xO_y@PEG$  (283 mM of NaCl and 8.5 mM of  $CaCl_2$ ) were higher than those for lower grafting  
37  
38 density of  $Mn_xO_y@OA$  (236 mM of NaCl and 11.2 mM of  $CaCl_2$ ) and  $Mn_xO_y@PEG$  (173 mM of  
39  
40 NaCl and 1.8 mM of  $CaCl_2$ ), respectively. We hypothesize that, higher grafting densities lead to  
41  
42 higher electrostatic and steric repulsion forces due to higher entropic restriction and osmotic  
43  
44 pressure difference(s), and thus consequently resulted in higher colloidal stability.<sup>37-39</sup> It should  
45  
46 be noted that aggregation kinetics for  $Mn_xO_y@CTAB$  were unfavorable under high NaCl (2000  
47  
48 mM) and  $CaCl_2$  (1000 mM) concentrations and therefore, stability based on CCC values could not  
49  
50 be compared (Fig. S3).  
51  
52  
53  
54  
55  
56  
57  
58  
59  
60

1  
2  
3  
4 Since NOM is ubiquitous in natural systems and can form complexes with metal oxides  
5  
6 in natural water, we further investigated the colloidal stability water stable NPs (with a varied  
7  
8 grafting densities) in the presence of humic acid (HA). For these systems, HA in water actually  
9  
10 improves the colloidal stability of NPs with low grafting density. In the presence of HA (1 mg  
11  
12 L<sup>-1</sup> TOC), phase-transferred NPs with low grafting density showed a significant increase in CCC  
13  
14 value in NaCl compared to the absence of HA. For Mn<sub>x</sub>O<sub>y</sub>@OA, the CCC for lower grafting  
15  
16 density in the presence of HA were 1325 mM of NaCl, which was substantially higher than 236  
17  
18 mM of NaCl in the absence of HA. In contrast, higher grafting density NPs had similar or slightly  
19  
20 higher CCC value (994 and 855 mM of NaCl in the presence or absence of HA, respectively).  
21  
22 Similar results were obtained for Mn<sub>x</sub>O<sub>y</sub>@PEG, where the CCC for lower grafting density showed  
23  
24 dramatic increase from 173 to 1372 mM of NaCl in the presence of HA. As observed in previous  
25  
26 studies, HA can improve colloidal stability of NPs once attached to their surface(s).<sup>40, 41</sup> Our  
27  
28 results show that the effect of HA on the stability of NPs is also a function of grafting density.  
29  
30 We hypothesize that HA can more readily attach to NPs with lower grafting density and effectively  
31  
32 improve their stability due to possible (increased) hydrophobic interactions.<sup>42</sup> While the CCC  
33  
34 values increased with HA as a function of NaCl concentration, HA actually enhanced aggregation  
35  
36 in the presence of calcium (Ca<sup>2+</sup>) through what is likely to be intermolecular bridging as shown by  
37  
38 others<sup>40</sup>, resulting in lower CCC values (5.75 and 5.45 mM of CaCl<sub>2</sub> for Mn<sub>x</sub>O<sub>y</sub>@OA and  
39  
40 Mn<sub>x</sub>O<sub>y</sub>@PEG, respectively). In addition, the slopes of attachment efficiency curves in the  
41  
42 presence of HA are steeper than those obtained in the absence of HA for all types of surface coating  
43  
44 evaluated. This observation was attributed by the adsorption of HA to NPs which can enhance  
45  
46 relatively aggregation kinetic sensitivity.<sup>43</sup>  
47  
48  
49  
50  
51  
52  
53

54  
55 In comparison to Mn<sub>x</sub>O<sub>y</sub>@OA and Mn<sub>x</sub>O<sub>y</sub>@PEG, positively charged NPs  
56  
57  
58  
59  
60

1  
2  
3  
4 (Mn<sub>x</sub>O<sub>y</sub>@CTAB) with varied grafting density, showed different behavior with regard to colloidal  
5 stability, especially with divalent cationic salt (CaCl<sub>2</sub>) and HA (Fig. 2(f)). The CCC of  
6 Mn<sub>x</sub>O<sub>y</sub>@CTAB for higher grafting density (3.7 mM) is lower than lower grafting density (6.3  
7 mM) in CaCl<sub>2</sub> with 1 mg L<sup>-1</sup> of HA. We expected positively charged functional groups could to  
8 more readily associate with negatively charged HA due to the electrostatic attraction, thus resulting  
9 in lower CCC in CaCl<sub>2</sub>. We verified that the D<sub>H</sub> of higher grafting density (129 nm) was larger  
10 than lower grafting density (94.8 nm) in the presence of HA, indicating more HA adsorbed on  
11 Mn<sub>x</sub>O<sub>y</sub>@CTAB with higher grafting density. For a higher concentration of HA (10 mg L<sup>-1</sup> TOC),  
12 the CCC values of both higher and lower grafting densities were similar (3.4 and 3.6 mM of CaCl<sub>2</sub>)  
13 as shown in Fig. 2(f). At such high concentration of HA, NPs are likely to be completely coated  
14 by HA regardless of grafting density, thus identical CCC values. Aggregation kinetics for  
15 Mn<sub>x</sub>O<sub>y</sub>@CTAB in 2000 mM of NaCl in the presence of HA is presented in Fig. 2(e). Here, the  
16 aggregation rate increased with increase of grafting density in the same concentration of HA,  
17 which are consistent with results obtained from aggregation kinetics as a function of CaCl<sub>2</sub>.  
18  
19  
20  
21  
22  
23  
24  
25  
26  
27  
28  
29  
30  
31  
32  
33  
34  
35  
36  
37  
38  
39

#### 40 **Transport behavior in water saturated porous media**

41  
42  
43 We performed column studies with water-saturated porous media to evaluate the transport  
44 behavior of Mn<sub>x</sub>O<sub>y</sub> NPs with different grafting densities. Breakthrough curves (BTCs) of  
45 effluent normalized by the influent concentration (C/C<sub>0</sub>) for Mn<sub>x</sub>O<sub>y</sub> NPs transport through water  
46 saturated columns are presented in Fig. 3. For comparison, representative BTCs for non-reactive  
47 (control) tracer were obtained, with C/C<sub>0</sub> reaching 1.0. In addition, tracer BTC shapes were  
48 consistent for all columns, with steep increase and decrease of C/C<sub>0</sub>, indicating ideal equilibrium  
49  
50  
51  
52  
53  
54  
55  
56  
57  
58  
59  
60

1  
2  
3  
4 transport behavior.<sup>30,44</sup> In contrast to tracer transport, BTCs for organic coated  $Mn_xO_y$  NPs never  
5 reached  $C/C_0 = 1$ , indicative of favorable particle-collector interactions. NP breakthrough then  
6  
7 showed gradually decreasing concentration after maximum relative concentration ( $C/C_0$ ) in all  
8  
9 types of surface stabilizers. This observation can indicate that significant portion of the NPs were  
10  
11 retained irreversibly in the column and the retained NPs were slowly released from the sand, which  
12  
13 is likely due to secondary minimum interactions between NPs and sand.<sup>45</sup> To capture NP release  
14  
15 behavior, measured BTCs were fit using the MFT method with a first-order detachment term.  
16  
17  
18 The tailing behavior observed in the experimental BTCs was successfully reproduced by the fitted  
19  
20 curves. The fitted detachment rates for all investigated conditions were two orders of magnitude  
21  
22 smaller than the attachment rates (Table S2), indicating minimal NP release compared to  
23  
24 attachment.  
25  
26  
27  
28  
29

30 The  $C/C_0$  of NPs with higher grafting density was similar or slightly higher than that of  
31  
32 lower grafting density in the absence of HA. Whether the grafting density of the engineered NPs  
33  
34 was high or low, all phase transferred NP samples were highly colloidally stable at low electrolyte  
35  
36 concentrations used in the column experiments (1 mM of KCl) and showed similar results. In  
37  
38 addition, the steric repulsion force for the bare sand could be lower than steric effects in  
39  
40 aggregation of NPs, resulting in relatively less impact of grafting density on their deposition  
41  
42 behavior. These results are similar to previous reports; the attachment efficiency of NPs to HA  
43  
44 coated silica surface is lower than that of NPs to bare silica surface due to additional steric  
45  
46 stabilization of HA on the silica surface.<sup>41</sup> Batch reactor experiments were also conducted  
47  
48 depending on the grafting density of the engineered NPs to provide the supporting evidence  
49  
50 regarding deposition behavior on sand (Table S1). Similar or higher  $C/C_0$  was achieved in higher  
51  
52 grafting density and  $Mn_xO_y@CTAB$  showed highest  $C/C_0$ , followed by  $Mn_xO_y@OA$  and  
53  
54  
55  
56  
57  
58  
59  
60



1  
2  
3  
4  $\text{Mn}_x\text{O}_y@$ PEG, which is consistent with their colloidal stabilities (and previously discussed results).

5  
6 The attachment efficiency ( $\alpha$ ) and single collector efficiency ( $\eta_0$ ) of NPs to the sand calculated  
7 using equation 2 and 3 are presented in Table 1. The resulting attachment efficiencies ( $\alpha$ ) were  
8 0.0115 for  $\text{Mn}_x\text{O}_y@$ OA, 0.0227 for  $\text{Mn}_x\text{O}_y@$ PEG, and 0.0127 for  $\text{Mn}_x\text{O}_y@$ CTAB, respectively.  
9 The MFT fitted parameters ( $k_{\text{att}}$ ,  $k_{\text{det}}$  and  $S_{\text{max}}$ ) for three  $\text{Mn}_x\text{O}_y$  nanoparticles at two grafting  
10 density were also similar (Table S2). For example, the fitted attachment rates for  $\text{Mn}_x\text{O}_y@$ OA,  
11  $\text{Mn}_x\text{O}_y@$ PEG, and  $\text{Mn}_x\text{O}_y@$ CTAB were 1.20-1.38, 1.79-1.82, 1.43-1.46 1/h at low and high  
12 grafting densities, respectively, indicating the surface coating density did not strongly influence  
13 the rate of NP attachment.  
14  
15  
16  
17  
18  
19  
20  
21  
22  
23  
24

25 We observed negligible effects of HA on the  $C/C_0$  for  $\text{Mn}_x\text{O}_y@$ OA and  $\text{Mn}_x\text{O}_y@$ PEG.

26 Both negatively charged NPs likely have sufficient electrostatic repulsion forces, with respect to  
27 HA, for low electrolyte concentration. This is supported by identical  $D_H$  regardless of HA for  
28  $\text{Mn}_x\text{O}_y@$ OA and  $\text{Mn}_x\text{O}_y@$ PEG as shown in Table 1. The MFT fitted  $S_{\text{max}}$  in the absence and  
29 presence of HA for  $\text{Mn}_x\text{O}_y@$ OA and  $\text{Mn}_x\text{O}_y@$ PEG were also similar ( $\sim 1.5 \mu\text{g/g}$  sand), indicating  
30 the minimal effect of HA on the attachment of negatively charged  $\text{Mn}_x\text{O}_y$ . In comparison, for  
31 positively charged  $\text{Mn}_x\text{O}_y@$ CTAB, the  $C/C_0$  significantly decreased in the presence of HA as also  
32 shown in Table 1 from 0.380 and 0.214 to 0.134 and 0.093 for higher and lower grafting densities,  
33 respectively. This result is consistent with the results of aggregation behavior in which HA  
34 adsorbs to the positively charged  $\text{Mn}_x\text{O}_y@$ CTAB and these larger aggregates were more likely to  
35 interact with a particle collector. We verified that the  $D_H$  of  $\text{Mn}_x\text{O}_y@$ CTAB NPs significantly  
36 increased with HA due to adsorption from 37.8 and 40.9 to 129 and 94.8 nm, respectively.  
37  
38  
39  
40  
41  
42  
43  
44  
45  
46  
47  
48  
49  
50

51 Attachment efficiencies ( $\alpha$ ) of  $\text{Mn}_x\text{O}_y@$ CTAB to the soil media were also increased from 0.0127  
52 and 0.0214 to 0.077 and 0.0647 for higher and lower grafting densities in the presence of HA,  
53  
54  
55  
56  
57  
58  
59  
60

1  
2  
3  
4 respectively (Table 1). The greater attachment in the presence of HA was also observed for MFT  
5 fitted  $k_{att}$  values, which increased from from 1.43 h<sup>-1</sup> to 3.2 h<sup>-1</sup>. For all organic coatings, the  
6  
7 BTCs occurred/peaked were relatively moved backward in presence of HA (the peak concentration  
8 arrival time was at higher pore volume). This shift could be attributed by the change of transport  
9 properties in soil column, as organic matter reduces the preferential transport in column.<sup>46, 47</sup>  
10  
11  
12  
13  
14  
15

16 To determine the retention profile of NPs in soil media, we measured their concentrations  
17 in sectioned segments of column (Fig. S4). As expected, the attached NPs were relatively more  
18 abundant in the first section of column (inlet) for all types of surface stabilizers, which is consistent  
19 with previous studies.<sup>30, 48</sup> In the presence of HA, the highest retained concentration was  
20 observed in the second section of column for Mn<sub>x</sub>O<sub>y</sub>@OA and Mn<sub>x</sub>O<sub>y</sub>@PEG. We hypothesize  
21 that HA was substantially adsorbed to the first section of soil column and thus preventing  
22 negatively charged Mn<sub>x</sub>O<sub>y</sub>@OA and Mn<sub>x</sub>O<sub>y</sub>@PEG from attaching to the sand. For  
23 Mn<sub>x</sub>O<sub>y</sub>@CTAB, however, retention of NPs was highest near the inlet and declined along the  
24 column, for which positively charged NPs could attach to the HA occupied on the collector surface.  
25  
26  
27  
28  
29  
30  
31  
32  
33  
34  
35  
36  
37  
38  
39  
40

### 41 **Enhanced sorption with higher grafting density**

42  
43 Finally, we evaluated chromate sorption performance of Mn<sub>x</sub>O<sub>y</sub> NPs with various grafting  
44 densities for different surface stabilizers (OA, PEG, and CTAB). Positively charged  
45 Mn<sub>x</sub>O<sub>y</sub>@CTAB showed enhanced chromate sorption performance compared to negatively charged  
46 Mn<sub>x</sub>O<sub>y</sub>@OA and Mn<sub>x</sub>O<sub>y</sub>@PEG as observed previously by our group and others (Fig. 4).<sup>16, 49</sup>  
47  
48 Further, for Mn<sub>x</sub>O<sub>y</sub>@CTAB, higher grafting density resulted in higher Cr(VI) sorption density as  
49 shown in Fig. 4(c). The sorption density was 21, 37, 42, 90, and 87 mg g<sup>-1</sup> (milligram of Cr per  
50  
51  
52  
53  
54  
55  
56  
57  
58  
59  
60

1  
2  
3  
4 gram of NPs) for 9k, 18k, 24k, 51k, and 74k of grafting densities, respectively. As the dominant  
5  
6 species of Cr(VI) at pH 7 is negatively charged  $\text{HCrO}_4^-$  and  $\text{CrO}_4^{2-}$ , such correlation between Cr(VI)  
7  
8 sorption density and grafting density of NPs is attributed to the increased number of favorable  
9  
10 functional groups, thus simply providing more adsorbing sites. The maximum sorption observed  
11  
12 at 51k and above, indicates steric hindrance plays a role at high(er) loadings. For negatively  
13  
14 charged NPs ( $\text{Mn}_x\text{O}_y@OA$  and  $\text{Mn}_x\text{O}_y@PEG$ ), while increasing grafting density plays critical role  
15  
16 for colloidal stability, as discussed above, it does not provide additional (direct) sorption sites for  
17  
18 negatively charged species. Sorption densities of  $\text{Mn}_x\text{O}_y@OA$  NPs were 23, 26, 20, and 23 mg  
19  
20  $\text{g}^{-1}$  for 36k, 47k, 60k, and 77k of grafting density, and  $\text{Mn}_x\text{O}_y@PEG$  NPs were 19, 15, 12, 12, 23,  
21  
22 11, 12, and 23 mg  $\text{g}^{-1}$  for 16k, 23k, 23k, 24k, 26k, 27k, 31k, 47k of grafting density, respectively.  
23  
24  
25  
26  
27  
28  
29  
30

## 31 **Conclusions**

32  
33  
34 In this work, we describe the effects of grafting density on the colloidal stability, transport,  
35  
36 and sorption behavior of the engineered  $\text{Mn}_x\text{O}_y$  NPs in water. Higher grafting densities lead to  
37  
38 improved colloidal stability due to increasing steric repulsion forces. The stability of NPs was  
39  
40 also dependent on HA with respect to grafting density. CCC (stability) values of negatively  
41  
42 charged NPs with lower grafting density significantly increased in the presence of HA, while  
43  
44 having negligible effects for NPs with higher grafting density. For positively charged NPs, more  
45  
46 HA associates with higher grafting densities due to enhanced electrostatic attraction, resulting in  
47  
48 decreasing CCC values, which is likely due to the intermolecular bridging in the presence of  
49  
50  $\text{CaCl}_2$ . Transport behavior was consistent with aggregation behavior regardless of grafting  
51  
52 density for negatively charged  $\text{Mn}_x\text{O}_y@OA$  and  $\text{Mn}_x\text{O}_y@PEG$ , whereas positively charged  
53  
54  
55  
56  
57  
58  
59  
60

1  
2  
3  
4 Mn<sub>x</sub>O<sub>y</sub>@CTAB had increased deposition in the presence of HA. In addition, higher grafting  
5  
6 density for Mn<sub>x</sub>O<sub>y</sub>@CTAB led to higher chromate sorption capacities, as additional (favorable)  
7  
8 functional groups provided more sorption sites. Taken together this work clearly highlight the  
9  
10 need for more precise NP synthesis protocols, including surface modification, which allow for  
11  
12 critical comparison(s) of fundamental behavior. As demonstrated here, NP deposition and  
13  
14 sorption behavior can strongly depend on surface density of stabilizing layers – a fact that remains  
15  
16 under appreciated in many direct (nano)particle comparison studies done in an environmental  
17  
18 context.  
19  
20  
21  
22  
23  
24  
25

## 26 **Acknowledgements**

27  
28  
29 This work is supported by U.S. Army Corps of Engineers (W912HZ-13-2-0009-P00001), the U.S.  
30  
31 National Science Foundation (CBET 1437820), and U.S. Department of Agriculture, NIFA (2018-  
32  
33 67021-28319). XRD measurements were made possible by a grant from the U.S. National  
34  
35 Science Foundation (EAR-1161543). TEM, DLS, ultracentrifugation, and ICP-OES were  
36  
37 provided by the Nano Research Facility (NRF) at Washington University in St. Louis.  
38  
39  
40  
41  
42  
43  
44  
45  
46

## 47 **References**

- 48  
49  
50  
51 1. S. Kango, S. Kalia, A. Celli, J. Njuguna, Y. Habibi and R. Kumar, Surface modification of  
52 inorganic nanoparticles for development of organic–inorganic nanocomposites—a review,  
53 *Progress in Polymer Science*, 2013, **38**, 1232-1261.  
54 2. R. A. Sperling and W. J. Parak, Surface modification, functionalization and bioconjugation  
55 of colloidal inorganic nanoparticles, *Philosophical Transactions of the Royal Society A*:  
56  
57  
58  
59  
60

- 1
  - 2
  - 3
  - 4
  - 5
  - 6
  - 7
  - 8
  - 9
  - 10
  - 11
  - 12
  - 13
  - 14
  - 15
  - 16
  - 17
  - 18
  - 19
  - 20
  - 21
  - 22
  - 23
  - 24
  - 25
  - 26
  - 27
  - 28
  - 29
  - 30
  - 31
  - 32
  - 33
  - 34
  - 35
  - 36
  - 37
  - 38
  - 39
  - 40
  - 41
  - 42
  - 43
  - 44
  - 45
  - 46
  - 47
  - 48
  - 49
  - 50
  - 51
  - 52
  - 53
  - 54
  - 55
  - 56
  - 57
  - 58
  - 59
  - 60
- Mathematical, Physical and Engineering Sciences*, 2010, **368**, 1333-1383.
3. M. A. Boles, D. Ling, T. Hyeon and D. V. Talapin, The surface science of nanocrystals, *Nature materials*, 2016, **15**, 141.
  4. D. Guo, G. Xie and J. Luo, Mechanical properties of nanoparticles: basics and applications, *Journal of physics D: applied physics*, 2013, **47**, 013001.
  5. R. P. Bagwe, L. R. Hilliard and W. Tan, Surface modification of silica nanoparticles to reduce aggregation and nonspecific binding, *Langmuir*, 2006, **22**, 4357-4362.
  6. C. Levard, E. M. Hotze, G. V. Lowry and G. E. Brown Jr, Environmental transformations of silver nanoparticles: impact on stability and toxicity, *Environmental science & technology*, 2012, **46**, 6900-6914.
  7. Y. Li, W. Zhang, J. Niu and Y. Chen, Surface-coating-dependent dissolution, aggregation, and reactive oxygen species (ROS) generation of silver nanoparticles under different irradiation conditions, *Environmental science & technology*, 2013, **47**, 10293-10301.
  8. W. Yantasee, C. L. Warner, T. Sangvanich, R. S. Addleman, T. G. Carter, R. J. Wiacek, G. E. Fryxell, C. Timchalk and M. G. Warner, Removal of heavy metals from aqueous systems with thiol functionalized superparamagnetic nanoparticles, *Environmental science & technology*, 2007, **41**, 5114-5119.
  9. X. Zhao, W. Liu, Z. Cai, B. Han, T. Qian and D. Zhao, An overview of preparation and applications of stabilized zero-valent iron nanoparticles for soil and groundwater remediation, *Water research*, 2016, **100**, 245-266.
  10. M. Shen, H. Cai, X. Wang, X. Cao, K. Li, S. H. Wang, R. Guo, L. Zheng, G. Zhang and X. Shi, Facile one-pot preparation, surface functionalization, and toxicity assay of APTS-coated iron oxide nanoparticles, *Nanotechnology*, 2012, **23**, 105601.
  11. F. He and D. Zhao, Manipulating the size and dispersibility of zerovalent iron nanoparticles by use of carboxymethyl cellulose stabilizers, *Environmental Science & Technology*, 2007, **41**, 6216-6221.
  12. T. Phenrat, N. Saleh, K. Sirk, H.-J. Kim, R. D. Tilton and G. V. Lowry, Stabilization of aqueous nanoscale zerovalent iron dispersions by anionic polyelectrolytes: adsorbed anionic polyelectrolyte layer properties and their effect on aggregation and sedimentation, *Journal of Nanoparticle Research*, 2008, **10**, 795-814.
  13. X. Li, J. J. Lenhart and H. W. Walker, Aggregation kinetics and dissolution of coated silver nanoparticles, *Langmuir*, 2011, **28**, 1095-1104.
  14. E. M. Hotze, T. Phenrat and G. V. Lowry, Nanoparticle aggregation: challenges to understanding transport and reactivity in the environment, *Journal of environmental quality*, 2010, **39**, 1909-1924.
  15. S. S. Lee, W. Li, C. Kim, M. Cho, B. J. Lafferty and J. D. Fortner, Surface functionalized manganese ferrite nanocrystals for enhanced uranium sorption and separation in water, *Journal of Materials Chemistry A*, 2015, **3**, 21930-21939.
  16. C. Kim, S. S. Lee, B. J. Lafferty, D. E. Giammar and J. D. Fortner, Engineered superparamagnetic nanomaterials for arsenic (V) and chromium (VI) sorption and separation: quantifying the role of organic surface coatings, *Environmental Science: Nano*, 2018, **5**, 556-563.
  17. Y. Huang and A. A. Keller, EDTA functionalized magnetic nanoparticle sorbents for cadmium and lead contaminated water treatment, *Water research*, 2015, **80**, 159-168.
  18. D. Selli, S. Motta and C. Di Valentin, Impact of surface curvature, grafting density and solvent type on the PEGylation of titanium dioxide nanoparticles, *Journal of Colloid and*

- 1  
2  
3  
4 *Interface Science*, 2019, **555**, 519-531.
- 5 19. J. Lin, H. Zhang, V. Morovati and R. Dargazany, PEGylation on mixed monolayer gold  
6 nanoparticles: Effect of grafting density, chain length, and surface curvature, *Journal of*  
7 *Colloid and Interface Science*, 2017, **504**, 325-333.
- 8 20. D. N. Benoit, H. Zhu, M. H. Lillierose, R. A. Verm, N. Ali, A. N. Morrison, J. D. Fortner,  
9 C. Avendano and V. L. Colvin, Measuring the grafting density of nanoparticles in solution  
10 by analytical ultracentrifugation and total organic carbon analysis, *Analytical chemistry*,  
11 2012, **84**, 9238-9245.
- 12 21. C. Kim and J. D. Fortner, Surface-Engineered Nanomaterials in Water: Understanding  
13 Critical Dynamics of Soft Organic Coatings and Relative Aggregation Density,  
14 *Environmental Science & Technology*, 2020, **54**, 13548-13555.
- 15 22. K. An, M. Park, J. H. Yu, H. B. Na, N. Lee, J. Park, S. H. Choi, I. C. Song, W. K. Moon  
16 and T. Hyeon, Synthesis of uniformly sized manganese oxide nanocrystals with various  
17 sizes and shapes and characterization of their T1 magnetic resonance relaxivity, *European*  
18 *Journal of Inorganic Chemistry*, 2012, **2012**, 2148-2155.
- 19 23. S. S. Lee, W. Li, C. Kim, M. Cho, J. G. Catalano, B. J. Lafferty, P. Decuzzi and J. D.  
20 Fortner, Engineered manganese oxide nanocrystals for enhanced uranyl sorption and  
21 separation, *Environmental Science: Nano*, 2015, **2**, 500-508.
- 22 24. K. L. Chen and M. Elimelech, Aggregation and deposition kinetics of fullerene (C60)  
23 nanoparticles, *Langmuir*, 2006, **22**, 10994-11001.
- 24 25. K. L. Chen, B. A. Smith, W. P. Ball and D. H. Fairbrother, Assessing the colloidal  
25 properties of engineered nanoparticles in water: case studies from fullerene C60  
26 nanoparticles and carbon nanotubes, *Environmental Chemistry*, 2010, **7**, 10-27.
- 27 26. R. C. Heath, *Basic ground-water hydrology*, US Geological Survey, 1983.
- 28 27. G. Grisak, W. Merritt and D. Williams, A fluoride borehole dilution apparatus for  
29 groundwater velocity measurements, *Canadian Geotechnical Journal*, 1977, **14**, 554-561.
- 30 28. B. M. Patterson, M. D. Annable, E. B. Bekele and A. J. Furness, On-line groundwater  
31 velocity probe: Laboratory testing and field evaluation, *Journal of contaminant hydrology*,  
32 2010, **117**, 109-118.
- 33 29. K.-M. Yao, M. T. Habibian and C. R. O'Melia, Water and waste water filtration. Concepts  
34 and applications, *Environmental science & technology*, 1971, **5**, 1105-1112.
- 35 30. Y. Li, Y. Wang, K. D. Pennell and L. M. Abriola, Investigation of the transport and  
36 deposition of fullerene (C60) nanoparticles in quartz sands under varying flow conditions,  
37 *Environmental science & technology*, 2008, **42**, 7174-7180.
- 38 31. N. Tufenkji and M. Elimelech, Correlation equation for predicting single-collector  
39 efficiency in physicochemical filtration in saturated porous media, *Environmental science*  
40 *& technology*, 2004, **38**, 529-536.
- 41 32. Y. Wang, M. D. Becker, V. L. Colvin, L. M. Abriola and K. D. Pennell, Influence of  
42 residual polymer on nanoparticle deposition in porous media, *Environmental science &*  
43 *technology*, 2014, **48**, 10664-10671.
- 44 33. G. Fritz, V. Schädler, N. Willenbacher and N. J. Wagner, Electrosteric stabilization of  
45 colloidal dispersions, *Langmuir*, 2002, **18**, 6381-6390.
- 46 34. C. Kim, S. S. Lee, K. T. Kwan, J. Lee, W. Li, B. J. Lafferty, D. E. Giammar and J. D.  
47 Fortner, Surface functionalized nanoscale metal oxides for arsenic(v), chromium(vi), and  
48 uranium(vi) sorption: considering single- and multi-sorbate dynamics, *Environmental*  
49 *Science: Nano*, 2020, **7**, 3805-3813.
- 50  
51  
52  
53  
54  
55  
56  
57  
58  
59  
60

- 1
- 2
- 3
- 4
- 5 35. C. Kim, J. Lee, D. Schmucker and J. D. Fortner, Highly stable superparamagnetic iron
- 6 oxide nanoparticles as functional draw solutes for osmotically driven water transport, *npj*
- 7 *Clean Water*, 2020, **3**, 8.
- 8 36. A. Prakash, H. Zhu, C. J. Jones, D. N. Benoit, A. Z. Ellsworth, E. L. Bryant and V. L.
- 9 Colvin, Bilayers as phase transfer agents for nanocrystals prepared in nonpolar solvents,
- 10 *ACS nano*, 2009, **3**, 2139-2146.
- 11 37. A. J. Worthen, V. Tran, K. A. Cornell, T. M. Truskett and K. P. Johnston, Steric
- 12 stabilization of nanoparticles with grafted low molecular weight ligands in highly
- 13 concentrated brines including divalent ions, *Soft Matter*, 2016, **12**, 2025-2039.
- 14 38. B. Vincent, J. Edwards, S. Emmett and A. Jones, Depletion flocculation in dispersions of
- 15 sterically-stabilised particles ("soft spheres"), *Colloids and Surfaces*, 1986, **18**, 261-281.
- 16 39. B. Peng, Z. Liu and Y. Jiang, Aggregation of DNA-grafted nanoparticles in water: The
- 17 critical role of sequence-dependent conformation of DNA coating, *The Journal of Physical*
- 18 *Chemistry B*, 2022, **126**, 847-857.
- 19 40. K. L. Chen and M. Elimelech, Influence of humic acid on the aggregation kinetics of
- 20 fullerene (C60) nanoparticles in monovalent and divalent electrolyte solutions, *Journal of*
- 21 *Colloid and Interface Science*, 2007, **309**, 126-134.
- 22 41. K. L. Chen and M. Elimelech, Interaction of fullerene (C60) nanoparticles with humic acid
- 23 and alginate coated silica surfaces: measurements, mechanisms, and environmental
- 24 implications, *Environmental science & technology*, 2008, **42**, 7607-7614.
- 25 42. B. Peng, P. Liao and Y. Jiang, Preferential interactions of surface-bound engineered single
- 26 stranded DNA with highly aromatic natural organic matter: Mechanistic insights and
- 27 implications for optimizing practical aquatic applications, *Water Research*, 2022, **223**,
- 28 119015.
- 29 43. M. Elimelech, J. Gregory and X. Jia, *Particle deposition and aggregation: measurement,*
- 30 *modelling and simulation*, Butterworth-Heinemann, 2013.
- 31 44. Y. Wang, Y. Li, J. D. Fortner, J. B. Hughes, L. M. Abriola and K. D. Pennell, Transport
- 32 and retention of nanoscale C60 aggregates in water-saturated porous media, *Environmental*
- 33 *science & technology*, 2008, **42**, 3588-3594.
- 34 45. Y. Tian, B. Gao, C. Silvera-Batista and K. J. Ziegler, Transport of engineered nanoparticles
- 35 in saturated porous media, *Journal of Nanoparticle Research*, 2010, **12**, 2371-2380.
- 36 46. H. Liu, D. M. Forsmann, C. Kjærsgaard, H. Saki and B. Lennartz, Solute transport
- 37 properties of fen peat differing in organic matter content, *Journal of environmental quality*,
- 38 2017, **46**, 1106-1113.
- 39 47. M. Larsbo, J. Koestel, T. Kätterer and N. Jarvis, Preferential transport in macropores is
- 40 reduced by soil organic carbon, *Vadose Zone Journal*, 2016, **15**.
- 41 48. Y. Han, G. Hwang, D. Kim, S. A. Bradford, B. Lee, I. Eom, P. J. Kim, S. Q. Choi and H.
- 42 Kim, Transport, retention, and long-term release behavior of ZnO nanoparticle aggregates
- 43 in saturated quartz sand: Role of solution pH and biofilm coating, *Water research*, 2016,
- 44 **90**, 247-257.
- 45 49. M. Kumari, C. U. Pittman Jr and D. Mohan, Heavy metals [chromium (VI) and lead (II)]
- 46 removal from water using mesoporous magnetite (Fe<sub>3</sub>O<sub>4</sub>) nanospheres, *Journal of colloid*
- 47 *and interface science*, 2015, **442**, 120-132.
- 48
- 49
- 50
- 51
- 52
- 53
- 54
- 55
- 56
- 57
- 58
- 59
- 60

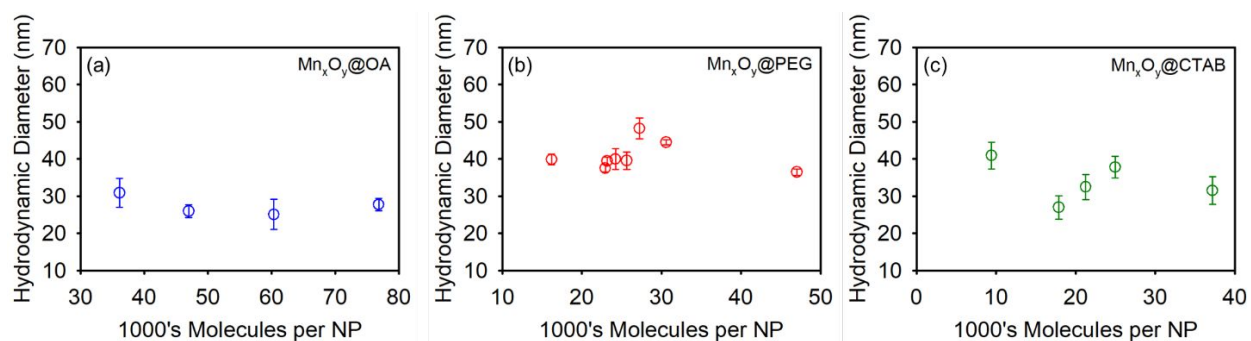
**Figures**

Figure 1. Hydrodynamic diameter ( $D_H$ ) of the surface functionalized manganese oxide nanoparticles ( $Mn_xO_y$  NPs) with different surface grafting densities at  $pH\ 7.0 \pm 0.2$ .  $Mn_xO_y$  NPs coatings include OA, PEG, and CTAB, here as: (a) $Mn_xO_y@OA$ , (b) $Mn_xO_y@PEG$ , and (c) $Mn_xO_y@CTAB$ .



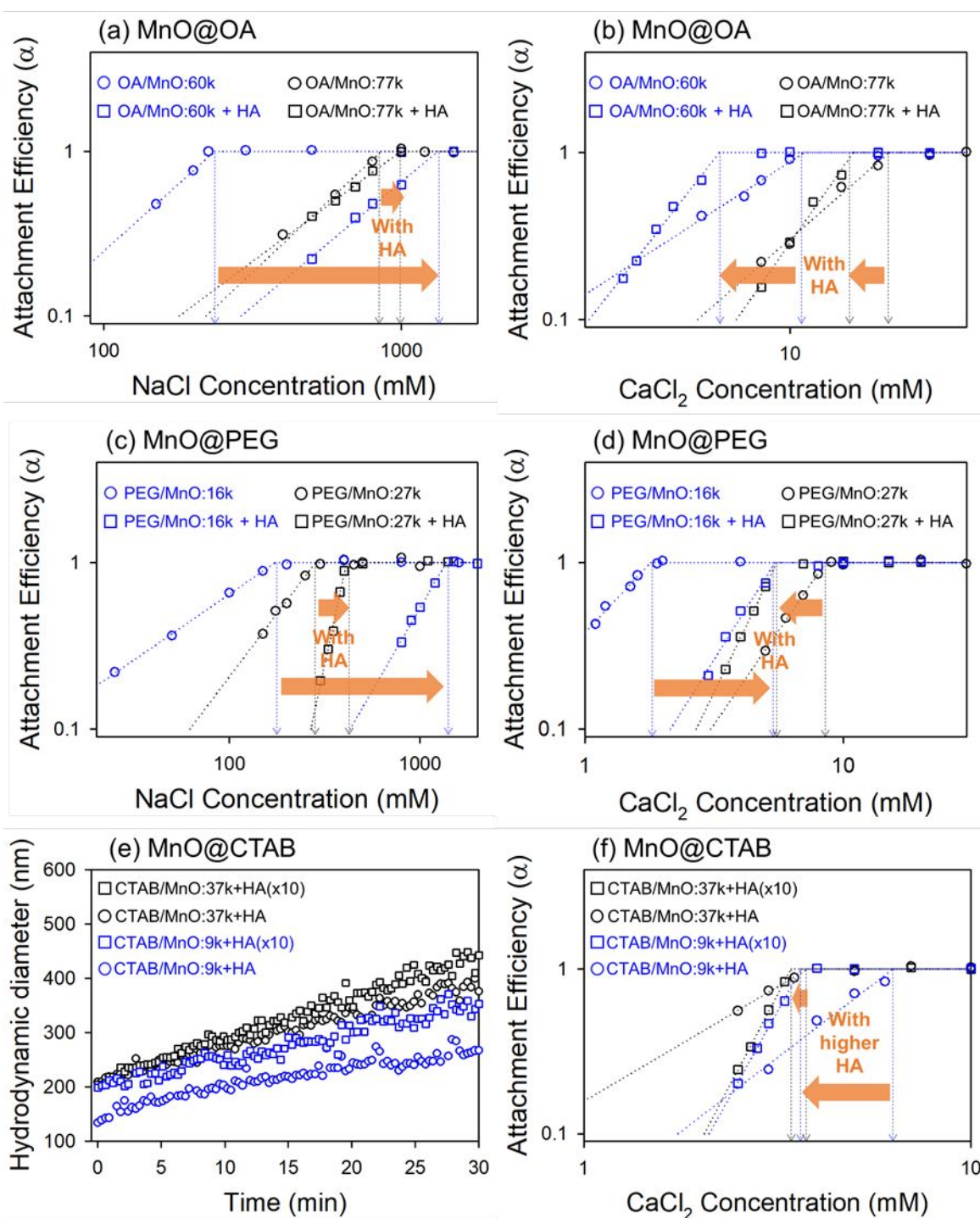


Figure 2. Attachment efficiency ( $\alpha$ ) of organic coated  $Mn_xO_y$  NPs with different grafting densities (e.g. OA/MnO:60k refers to 60k molecules of OA per MnO of nanocrystals) as a function of NaCl and  $CaCl_2$  concentrations in the absence and presence of humic acid (HA, 1 ppm) at pH

1  
2  
3  
4  $7.0 \pm 0.2$ ; (a-b)  $\text{Mn}_x\text{O}_y@OA$ , (c-d)  $\text{Mn}_x\text{O}_y@PEG$ , and (f)  $\text{Mn}_x\text{O}_y@CTAB$ . (e) Aggregation  
5  
6 profiles of  $\text{Mn}_x\text{O}_y@CTAB$  NPs with different grafting densities in the presence of humic acid (HA)  
7  
8 under 2 M of NaCl concentration.  
9  
10  
11  
12  
13  
14  
15  
16  
17  
18  
19  
20  
21  
22  
23  
24  
25  
26  
27  
28  
29  
30  
31  
32  
33  
34  
35  
36  
37  
38  
39  
40  
41  
42  
43  
44  
45  
46  
47  
48  
49  
50  
51  
52  
53  
54  
55  
56  
57  
58  
59  
60

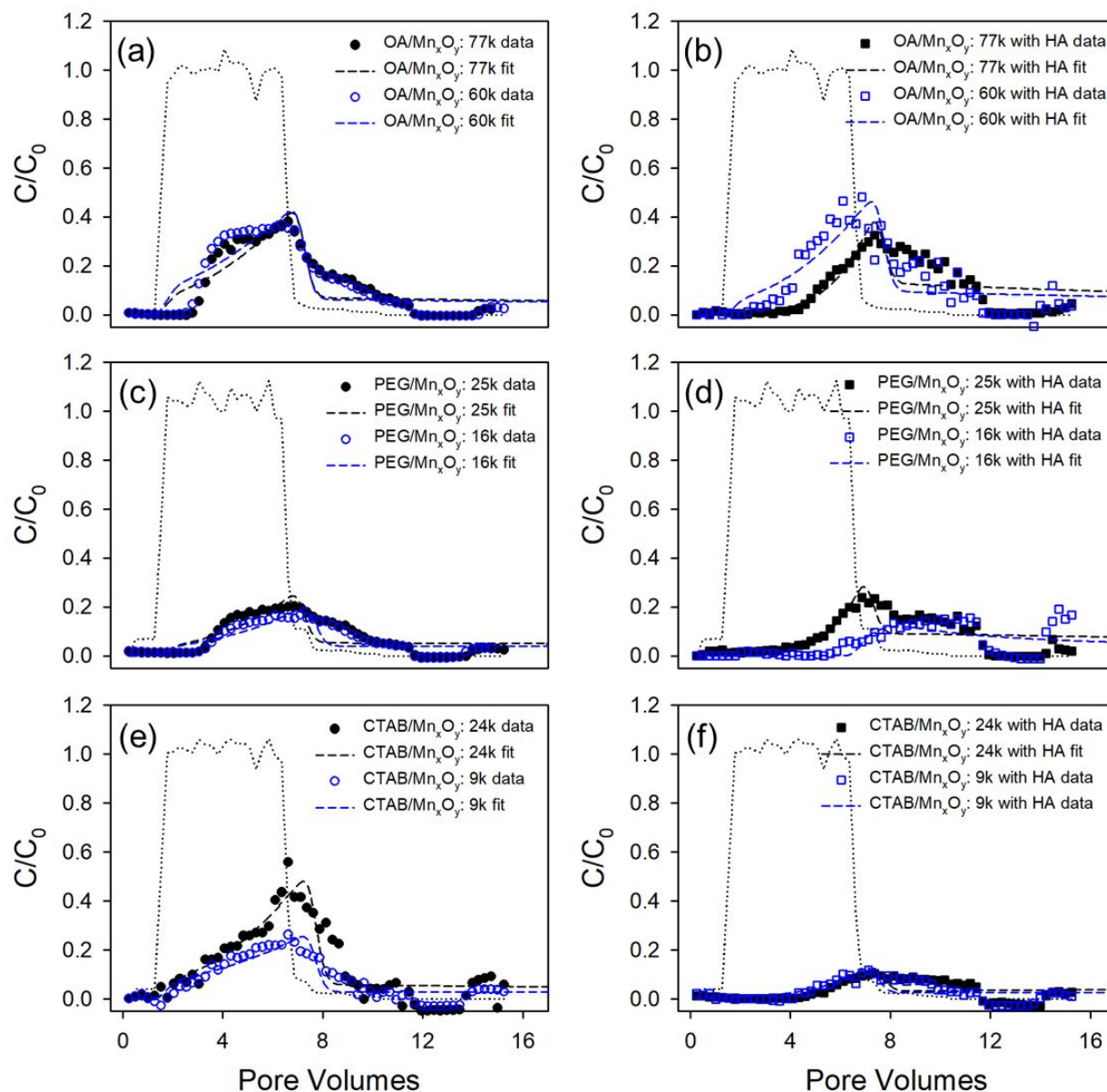


Figure 3. Experimental and fitted breakthrough curves (BTCs) of  $\text{Mn}_x\text{O}_y$  NPs with different grafting densities in water saturated columns packed with 30-40 mesh Ottawa sand in the absence and presence of HA; (a-b)  $\text{Mn}_x\text{O}_y@OA$ , (c-d)  $\text{Mn}_x\text{O}_y@PEG$ , and (e-f)  $\text{Mn}_x\text{O}_y@CTAB$ . All column experiments were performed at 0.76 m/d of a pore-water velocity and  $\text{pH } 7.0 \pm 0.2$ .

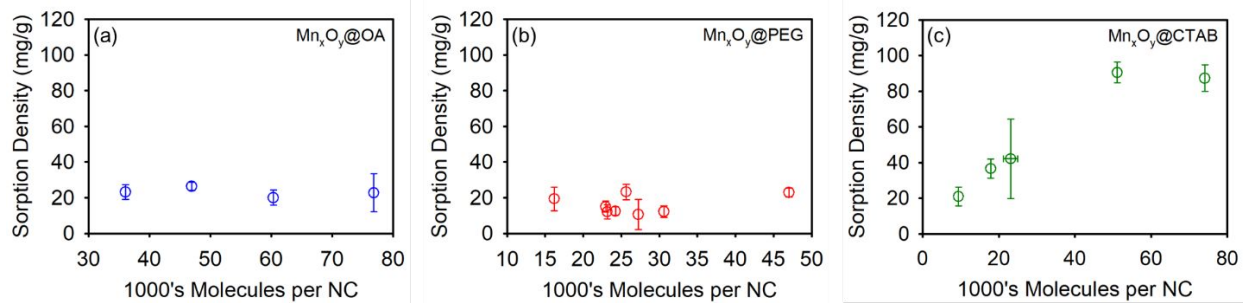


Figure 4. Sorption density of organic coated  $Mn_xO_y$  NPs as a function of grafting density (1000's molecules per NC) for different surface coatings; (a)  $Mn_xO_y@OA$ , (b)  $Mn_xO_y@PEG$ , and (c)  $Mn_xO_y@CTAB$ . Every test was conducted in the presence of 10 mg/L of  $Cr(VI)$  at  $pH 7.0 \pm 0.2$ .

Table 1. Single collector efficiency ( $\eta_0$ ) and attachment efficiency ( $\alpha$ ) of  $Mn_xO_y$  NPs with different grafting density.

Surface Stabilizer	Grafting Density	Hydrodynamic Diameter (nm)	Single Collector Efficiency ( $\eta_0$ )	Relative Concentration ( $C/C_0$ )	Attachment Efficiency ( $\alpha$ )
In the absence of HA					
OA	77k	27.8	0.36	0.33	0.012
	60k	25.1	0.39	0.33	0.010
PEG	25k	39.5	0.27	0.19	0.023
	16k	39.9	0.27	0.16	0.025
CTAB	24k	37.8	0.28	0.38	0.013
	9k	40.9	0.27	0.22	0.021
In the presence of HA					
OA	77k	28.7	0.35	0.30	0.013
	60k	29.2	0.36	0.36	0.011
PEG	25k	38.2	0.28	0.28	0.017
	16k	37.8	0.28	0.28	0.017
CTAB	24k	129	0.11	0.13	0.070
	9k	94.8	0.14	0.09	0.065